BIWIC 2016

23rd International Workshop
on
Industrial Crystallization

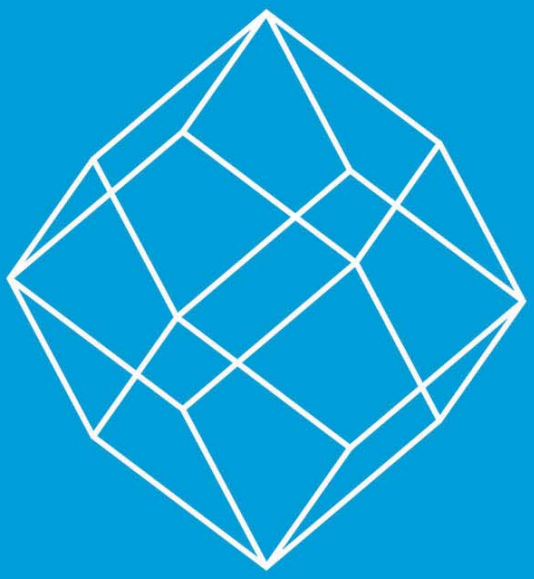

September 6 – 8, 2016

Max Planck Institute for Dynamics of
Complex Technical Systems
Magdeburg – Germany

Edited by
Heike Lorenz and Hannes Buchholz

Cuvillier Verlag Göttingen
Internationaler wissenschaftlicher Fachverlag

BIWIC 2016

23rd International Workshop on Industrial Crystallization

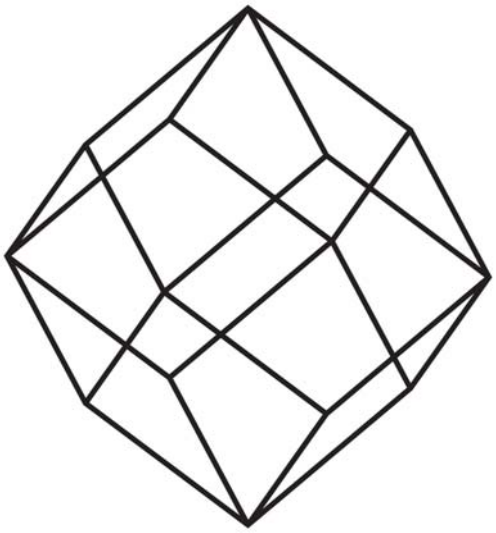

September 6 – 8, 2016

Max Planck Institute for Dynamics of
Complex Technical Systems
Magdeburg - Germany

Edited by

Heike Lorenz

and

Hannes Buchholz

Max Planck Institute for Dynamics of Complex Technical Systems
Magdeburg, Germany

Bibliografische Information der Deutschen Nationalbibliothek
Die Deutsche Nationalbibliothek verzeichnet diese Publikation in der Deutschen Nationalbibliografie; detaillierte bibliografische Daten sind im Internet über http://dnb.d-nb.de abrufbar.
1. Aufl. - Göttingen: Cuvillier, 2016

Nonnenstieg 8, 37075 Göttingen
Telefon: 0551-54724-0
Telefax: 0551-54724-21
www.cuvillier.de

1. Auflage, 2016
Gedruckt auf umweltfreundlichem, säurefreiem Papier aus nachhaltiger Forstwirtschaft.

ISBN 978-3-7369-9322-8
eISBN 978-3-7369-8322-9

Preface

Crystallization is a key technology for separation and purification of substances as well as for product design in chemical and life-science industries. Amounts of crystalline products range from several kg to multi-ton scales per year taking into account highly active pharmaceuticals on the one side and bulk chemicals such as inorganic salts for fertilizer applications on the other side. In addition, in topics of social interest, such as sustainability, crystallization processes become more and more important both in research and practice.

The main topics of the 23rd BIWIC reflect key applications as well as recent trends & challenges of crystallization, thus covering:

- Fundamentals of crystallization
- Separation, purification and formulation in life-science industries with applications in food, pharmaceuticals and agrochemicals sectors
- Monitoring and modeling of crystallization processes
- Crystallization for sustainability

It is our pleasure to host the BIWIC in 2016 for the second time after 2008 at the Max Planck Institute for Dynamics of Complex Technical Systems in Magdeburg. It is already the 23rd workshop after being established by Joachim Ulrich in Bremen in 1990 and continues successful events held in the last years in Halle, Delft, Tianjin, Odense, Rouen and Daejeon.
It brings together every year scientists and engineers from academia and industry, experts as well as newcomers, to present and discuss their current work and also to identify challenging fields of research of both fundamental and industrial interest. This year's participants come from 20 countries showing that the BIWIC has become a real international forum of the crystallization community. The particularly informal atmosphere offers plenty of opportunities for PhD students to exchange experiences, initiate collaborations and to get in contact with international experts.

We would like to thank the members of the scientific and organizing committees for their active and continuous support in the preparation of the workshop. Our special thanks go to Joachim Ulrich for again offering us the opportunity to organize and hold the BIWIC in Magdeburg. Finally, the valuable contributions from industry, financial support and inspiring scientific presentations, are gratefully acknowledged.

We wish all the participants a fruitful and enjoyable workshop and a memorable BIWIC 2016,

Heike Lorenz and Hannes Buchholz

Crystallization Team
Physical and Chemical Foundations of Process Engineering
Max Planck Institute for Dynamics of Complex Technical Systems
Magdeburg, July 2016

Scientific Committee

Jens-Petter Andreassen (Trondheim, Norway)
Jianxin Chen (Tianjin, China)
Gérard Coquerel (Rouen, France)
Adrian Flood (Nakhon Ratchasima, Thailand)
Izumi Hirasawa (Tokyo, Japan)
Kwang-Joo Kim (Daejeon, South Korea)
Herman Kramer (Delft, The Netherlands)
Alison Lewis (Cape Town, South Africa)
Heike Lorenz (Magdeburg, Germany), Chair
Marjatta Louhi-Kultanen (Lappeenranta, Finland)
Haiyan Qu (Odense, Denmark)
Andreas Seidel-Morgenstern (Magdeburg, Germany)
Joachim Ulrich (Halle, Germany)

Organizing Committee

Heike Lorenz
Sophia Pistorius
Gabriele Ebel
Jan Protzmann
Hannes Buchholz
Stephan Münzberg
Erik Temmel

Organizing Committee and Crystallization Team at the Max Planck Institute Magdeburg

Content

Formic Acid (FA)/ Water Phase Diagram by Means of Temperature-Resolved Second Harmonic Generation and FA Phase Transition: A Reinvestigation

S. Clevers, L. Yuan, V. Dupray, G. Coquerel

Normandie Univ, Laboratoire SMS-EA3233, Univ Rouen, F76821, Mont Saint Aignan, France
valerie.duray@univ-rouen.fr

Temperature resolved second harmonic generation (TR-SHG) is used to investigate the Formic Acid (FA)/Water binary phase diagram. Beyond the redetermination of the eutectic temperature and composition (-52°C and 40wt% in water, respectively) we disambiguated the polymorphic transition of FA suspected in the literature but never confirmed. Indeed, FA cannot be obtained as pure component and contains always a small amount of water. We propose that anomalies detected by IR and Raman spectroscopies are due to eutectic reaction rather than a genuine polymorphic transition.

1 Introduction

Second Harmonic Generation (SHG) is a nonlinear optical process that occurs in crystal with non-centrosymmetric (NC) space groups. It was proposed as an efficient technique for pre-screening of conglomerate [1] and to probe the structural purity reaching a detection threshold at the ppm level [2]. Temperature Resolved SHG (TR-SHG) has already been employed to monitor solid–solid transitions [3] and to monitor in situ the crystallization of a NC phase from a supersaturated solution [4]. Recently the potential of SHG was successfully used to investigate the Urea/Water phase diagram.[5]. In this scope, we propose to reinvestigate the formic acid (FA)/water binary phase diagram by means of TR-SHG.

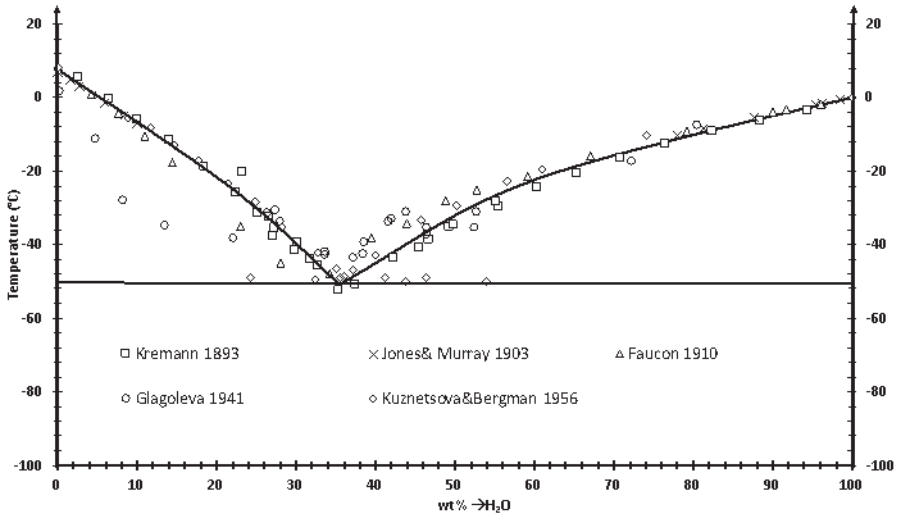

Fig 1: Binary formic acid/water phase diagrams found in literature taken from [6].

1.1 Presentation of the formic acid/ water system

Intensive research in literature was performed to find existing phase diagram of formic acid/water system and entries are plotted in Fig 1 taken from [6]. One can notice that the original papers were not found with consequently unknown information about the experimental conditions and purities. Data from the various authors seem in agreement

except for the Glagoleva's values. This discrepancy could be explained by measurements performed only upon cooling. From Kuznetsova & Bergman and Kremann data, the eutectic temperature T_E was determined at -49.5°C and -52.5°C, respectively. The eutectic composition was determined at circa 36 wt% of water (*i.e.* circa 59 % mol. of water). It is worth noting that in many studies as in our work, the FA used was not totally pure and often contained small amounts of water Obtaining very pure FA is difficult since it decomposes spontaneously into water and carbon monoxide [7,8] and also due to its hygroscopic behaviour. These features induce slight changes in the mixture compositions and could be a source of discrepancy.

1.2 Polymorphism in Formic Acid

Concerning possible polymorphism and solid-solid transition of formic acid, the literature remains unclear on some aspects. The study of formic acid in the solid state started as early as 1924 with the beginning of X-Ray diffraction [9] but the first crystal structure was only resolved in 1953 by Single Crystal X-Ray Diffraction (SC-XRD) at 223K. FA crystallizes in the NC space group $P\mathrm{na}2_1$ [10]. This space group was confirmed by other SC-XRD, XRPD and neutron diffractions experiments [11,12]. More recently studies performed under various pressure by SC-XRD highlighted a phase transition at 0.8GPa toward a centrosymmetric *P*nma polymorph[13]. However, other XRPD studies at high pressure up to 12 GPa reveal no structural transition (maintenance of LT form) [14]. On the basis of X-Ray and neutron diffraction the $P\mathrm{na}2_1$ form is stable from 4.5K to the melting point (281K) under ambient pressure. Nevertheless, polymorphism of crystalline FA at ambient pressure has been suspected in the literature based notably on Infrared (IR) because of splitting of infrared bands but also on Raman and DSC analyses[15-21]. Thereupon, a first-order transition was proposed and detected at -66°C upon cooling and circa -55°C upon heating by Zelsmann *et al* and -53°C by Grip *et al.* These discrepancies between crystallographic, spectroscopic and thermal data on possible polymorphism of FA have never been explained.

2 Experimental Methods

2.1 Materials

Samples of $HCOOH/H_2O$ mixtures were prepared using 98%-100% Formic Acid supplied by Fisher Chemical (CAS 64-18-6) and Milli-Q water without further purification. Karl-Fischer titration performed on commercial FA reveals the presence of circa 0.5wt% of water.

2.2 Temperature Resolved Second Harmonic Generation (TR-SHG)

Fig. 2 shows the experimental setup used for the TR-SHG measurements. A Nd:YAG Q-switched laser (Quantel) operating at 1.06 μm was used to deliver up to 360 mJ pulses of 5 ns duration with a repetition rate of 10 Hz. An energy adjustment device made up of two polarizers (P) and a half-wave plate (λ/2) allowed the incident energy to vary from 0 to ca. 200 mJ per pulse. A RG1000 filter was used after the energy adjustment device to remove light from laser flash lamps. The samples (few mg) were placed in a computer controlled Heating-Cooling stage (Linkam THMS-600) and were irradiated with a laser beam (4 mm in diameter). The signal generated by the sample (diffused light) was collected into an optical fiber (500 μm of core diameter) and directed onto the entrance slit of a spectrometer (Ocean Optics). A boxcar integrator allowed an average spectrum (spectral range 490-590 nm) with a resolution of 0.1 nm to be recorded over 3 s (30 pulses).

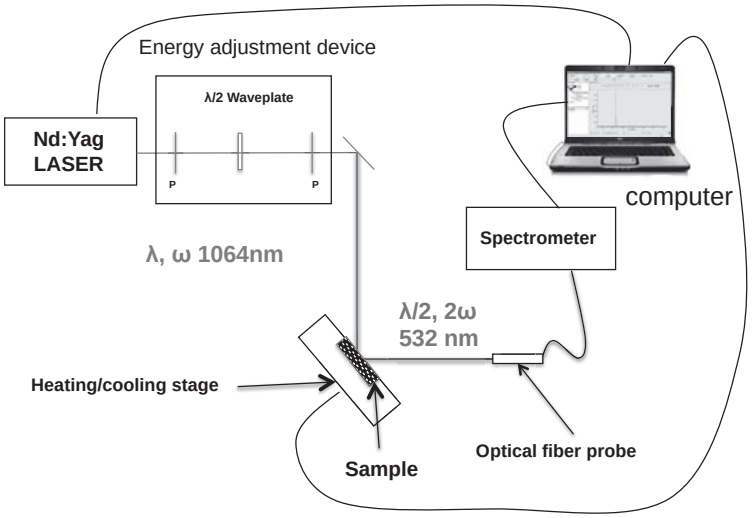

Fig. 2: Experimental setup Second Harmonic Generation Apparatus constituted of Nd:YAG Q-switched laser operating at 1064 nm.

According to Kurtz and Perry SHG powder method [22], SHG signal intensities were compared to the signal of a reference compound (α-quartz powder- 45 μm average size).

2.3 Differential Scanning Calorimetry (DSC)

Thermal analyses of the solids were conducted on DSC 204 F1 Netzsch equipped with an Intracooler. Solid samples (mass of c.a 15 mg with maximum deviation of 0.05mg) were placed in a 25 μL close aluminum crucible. The atmosphere of the analyses was regulated by Helium flux (40 $mL.min^{-1}$), and heat runs were conducted at different constant heating rate. The data treatment was performed with the Netzsch–TA Proteus ® Software v 4.8.4.

3 Results and Discussion

3.1 Theoretical hypothesis on the evolution of SHG signal in binary system

Possibly, several cases are imaginable depending on the nature of pure A and B crystals and of their equilibrium. In the following, we assume that the compound A crystallizes in a non-centrosymmetric space group and B in a centrosymmetric one. Moreover, it is supposed that no solid-solid phase transition occurs during heating. In addition, the theory is developed here only for a simple eutectic phase diagram. The theoretical evolution for the SHG signal in a binary eutectic mixture of A and B at given composition (rich in A) during the heating is plotted on Fig. 3.

In the domain rich in NC phase, the theoretical evolution of the SHG signal (composition I) could be described by: (1) an evolution of the SHG efficiency with the temperature (mainly related to the evolution of nonlinear properties of <A> crystal with temperature). Due to phase matching properties, the SHG signal could remain stable, increase or decrease with temperature, (2) at the eutectic temperature T_E, a sharp decrease of the SHG signal should occur because of the appearance of the liquid phase due to the scattering and/or the absorption of the liquid and the melting of the eutectic microstructure (It has been shown that in favourable cases, eutectic microstructures can highly contribute to the SHG signal through a quasi-phase matching process[23]), (3) A progressive decrease of SHG signal due to the disappearance of <A> crystals upon heating. (4) The complete vanishing of the SHG signal corresponds to the liquidus temperature T_L. The sample is then totally liquid and the SHG signal remains null (5) upon further heating.

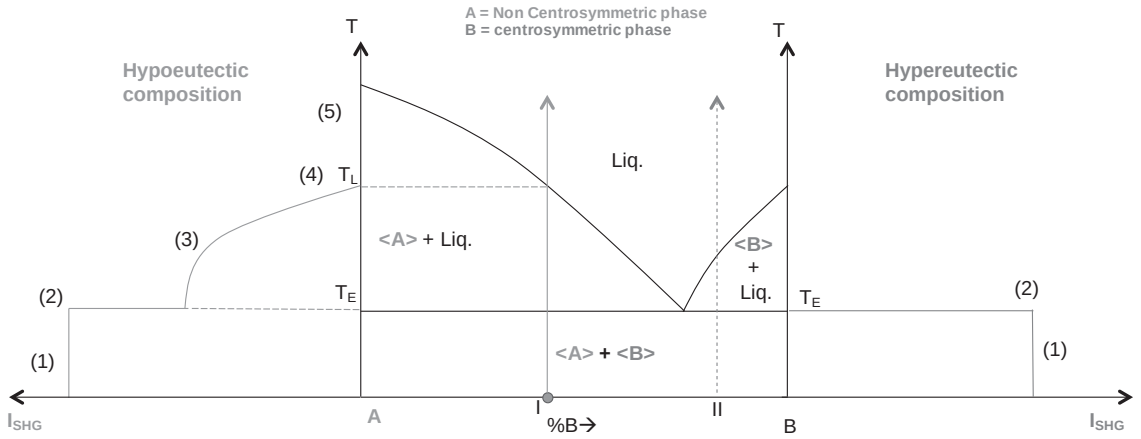

Fig. 3: Theoretical TR-SHG curve for A/B mixture in the hypoeutectic composition (NC phase rich composition), left and the hypereutectic composition (right)

The same assumptions are valid for enriched B mixtures (hypereutectic part) leading to a sharp decrease of the SHG signal at the eutectic temperature (2). By contrast to hypoeutectic mixtures, the signal should totally vanish because the system is then only composed of centrosymmetric phases (liquid and <B> crystals). By repeating these experiments for several compositions, it is thus possible to plot the liquidus and the eutectic lines. These hypotheses were confirmed through the investigation of the formic acid/water binary system.

3.2 Formic Acid/ Water binary phase diagram

Several mixtures of formic acid and water (total mass of 10 g) were prepared and analysed by TR-SHG. Firstly, the sample was cooled to -100°C at 2K/min and then heated at 1K/min with SHG measurements performed upon heating every 1 or 2 minutes (consequently the error on the temperature is approximately 0.05°C for a measurement duration of 3sec). TR-SHG results are detailed for only one hypoeutectic and one hypereutectic composition. Fig. 4 shows the TR-SHG curves obtained for 80/20 and 50/50(%wt.) compositions and it appears that the experimental results fit pretty well the elaborated theory.

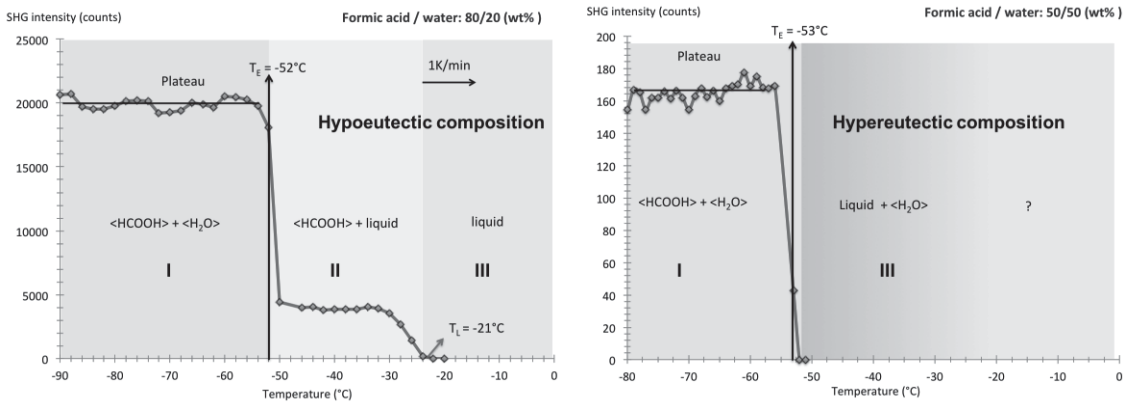

Fig. 4: (left) TR-SHG curve for 80/20 (wt%) mixture at 1K.min-1. Domains are determined from SHG signal interpretations: mixture of ice and formic acid crystal (I); mixture of formic acid crystal and liquid (II); pure liquid (III). (right) TR-SHG curve for 50:50 (wt.%) composition. Only the eutectic temperature is detected and above TE, the SHG signal totally vanishes meaning that the investigated mixture is centrosymmetric (<ice> + liquid binary domain).

For hypoeutectic 80/20 composition, positive SHG signal is detected at -100°C confirming the non-centrosymmetric nature of the sample (attributed in this case to formic acid crystals that exhibits a SHG signal 20 times higher than quartz reference). The SHG signal remains relatively stable from -100°C to -53°C. At circa -52°C, the signal decreases sharply (divided by four) and after decreases progressively to totally vanish at -21°C. For hypereutectic composition 50/50, only the eutectic temperature is detected (at circa -53°C), then the signal completely vanishes. It means that above -53°C, the system is totally centrosymmetric (*i.e.* only composed of liquid and water crystals).

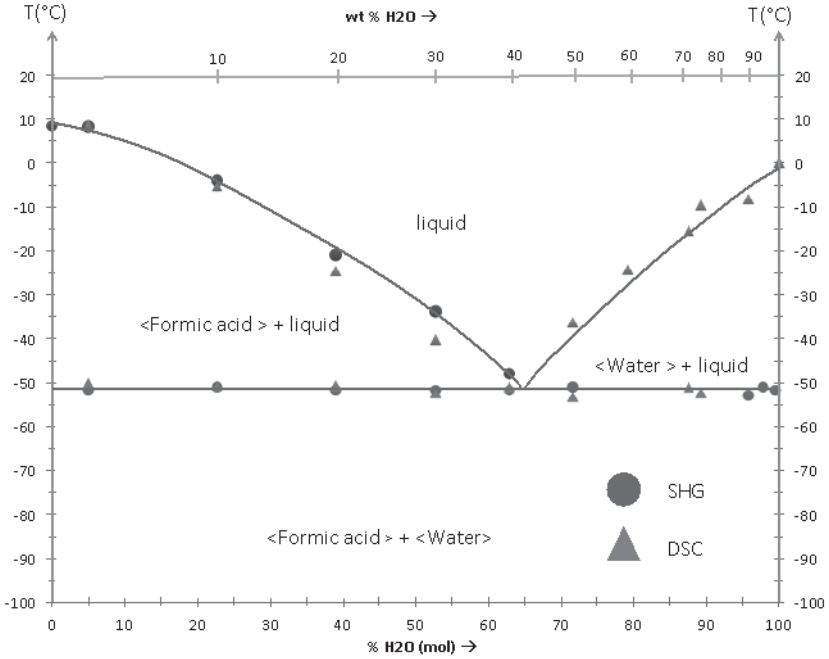

Fig. 5: Formic Acid/ Water phase diagram from TR-SHG (blue circles) and DSC (orange triangles) data.

DSC analyses were performed for the same compositions at 1K/min in order to compare the thermal analysis data to the TR-SHG results. To determine the eutectic and liquidus temperatures, the onset and the peak temperature are taken on the DSC chart, respectively. The phase diagram gathering DSC and TR-SHG results is plotted Fig. 5**.** The eutectic composition was determined at circa 40 wt% in water and T_E at circa -52°C. Eutectic temperatures determined by both TR-SHG and DSC are relatively close, nevertheless some differences in the liquidus temperatures are observed and are all the more pronounced that the water concentration is high. In this matter, DSC analyses can suffer of a lack of precision since it is difficult to decouple eutectic and liquidus endotherms for compositions close to the eutectic composition (due the shape of the liquidus peak). For instance, DSC chart for the composition 60/40 only presents one peak although it is possible to differentiate eutectic and liquidus temperature by TR-SHG. Results are in agreement with literature.

4 Conclusions

Through the investigation of the formic acid/ water binary phase diagram, the TR-SHG technique reveals its usefulness to the rapid and sensitive determination of phase domains boundaries. The main limitation of the TR-SHG technique is the impossibility to fully investigate the phase diagram in water rich compositions due to the centrosymmetric crystal structure of water. Nevertheless, it is of particular interest because it

serves to accurately discriminate the hypereutectic and hypoeutectic compositions. Therefore it gives the possibility to refine the eutectic compositions as demonstrated in a recent study[5]. In addition to the determination of the eutectic composition –circa 40% mass in water-, an important result is the determination of the eutectic temperature at circa -52°C. The eutectic endotherm on DSC charts is visible even for small amount of water. Moreover, at the eutectic temperature a sharp decrease is visible on the TR-SHG curves. These results and observations are of particular importance if we recall that phase transition was suspected at circa the same temperature than the eutectic invariant. It is not that surprising since formic acid free of water traces is difficult to obtained. Consequently, the optical anomalies on Raman and IR spectra and on the endotherm on DSC chart reported in literature could be explained by the detection of the eutectic invariant (*i.e.* the appearance of the liquid phase upon heating could explain these phenomena) and thus should not be associated to any polymorphic transition.

References

(1) A. Galland, V. Dupray, B. Berton, S. Morin-Grognet, M. Sanselme, H. Atmani, G. Coquerel, Crystal Growth & Design 9 (2009) 2713–2718.
(2) S. Clevers, F. Simon, V. Dupray, G. Coquerel, Journal of Thermal Analysis and Calorimetry (2013) 1–7.
(3) S. Clevers, F. Simon, M. Sanselme, V. Dupray, Crystal Growth & Design (2013) 3697–3704.
(4) D.J. LeCaptain, K.A. Berglund, Journal of Crystal Growth 203 (1999) 564–569.
(5) L. Yuan, S. Clevers, N. Couvrat, Y. CARTIGNY, V. Dupray, G. Coquerel, Chemical Engineering &Amp; Technology (n.d.).
(6) J. Timmermans, The Physico-Chemical Constants of Binary Systems in Concentrated Solutions, Volume 4: Systems with Inorganic+Organic or Inorganic Compounds, 1960.
(7) A.I. Popov, J.C. Marshall, Journal of Inorganic and Nuclear Chemistry 19 (1961) 340–347.
(8) M. Schmeißer, J. Schuster, arXiv Preprint arXiv:1108.5891 (2011).
(9) R.E. Gibbs, J. Chem. Soc., Trans. 125 (1924) 2622–2625.
(10) F.V. Holtzberg, B. Post, I. Fankuchen, Acta Cryst 6 (1953) 127–130.
(11) I. Nahringbauer, Acta Crystallogr B Struct Sci 34 (1978) 315–318.
(12) A. Albinati, K.D. Rouse, M.W. Thomas, Acta Crystallogr B Struct Crystallogr Cryst Chem 34 (1978) 2188–2190.
(13) D.R. Allan, S.J. Clark, Physical Review Letters 82 (1999) 3464.
(14) H. Yamawaki, S. Hawata, M. Sakashita, H. fujihisa, K. Aoki, High- Pressure Structures of Formic and Acetic Acids, Universities Press, 2000.
(15) R.C. Millikan, K.S. Pitzer, J. Am. Chem. Soc. 80 (1958) 3515–3521.
(16) Y. Mikawa, J. Chem. Phys. 45 (1966) 4750.
(17) Y. Mikawa, J.W. Brasch, R.J. Jakobsen, Journal of Molecular Spectroscopy 24 (1967) 314–329.
(18) R.J. Jakobsen, Y. Mikawa, J.W. Brasch, Spectrochimica Acta Part a: Molecular Spectroscopy 23 (1967) 2199–2209.
(19) H.R. Zelsmann, F. Bellon, Y. Marechal, B. Bullemer, Chemical Physics Letters 6 (1970) 513–515.
(20) J. Grip, E.J. Samuelsen, Phys. Scr. 24 (1981) 52–56.
(21) G.N. Robertson, M.C. Lawrence, Chemical Physics 62 (1981) 131–144.
(22) S.K. Kurtz, T.T. Perry, J. Appl. Phys. 39 (1968) 3798–3813.
(23) F. Simon, S. Clevers, G. Gbabode, N. Couvrat, V. Agasse-Peulon, M. Sanselme, V. Dupray, G. Coquerel, Crystal Growth & Design (2015) 150107130629001.

Thermal deformations of the crystal structures of L-valine, L-isoleucine and discrete compound V_2I

A. Isakov[1], E. Kotelnikova[1], S. Bocharov[1], A. Zolotarev Jr[1], H. Lorenz[2]

[1]Saint Petersburg State University, St. Petersburg, Russia
[2]Max Planck Institute for Dynamics of Complex Technical Systems, Magdeburg, Germany
kristallspbgu@mail.ru

Thermal behavior of three phases formed in the system valine—isoleucine was studied by means of temperature-resolved powder diffractometry. Samples were untreated reactants of Val and Ile and precipitate of the discrete compound V_2I crystallized from aqueous solution. Investigations were performed from room temperature until substance decomposition temperatures. Thermal deformations of the crystal structures were investigated for all studied phases: parameters of tensor of thermal deformations were calculated and figures of coefficients of thermal expansion of crystal structure were created.

1 Introduction

Thorough understanding of the nature of interrelations between solid phases in binary (solid—solid) chiral systems is a basis for effective using and improving the methods of isolation and separation of biochemically active chiral substances. When components of such a systems can undergo polymorph transformations, which can be further complicated by formation of non-equimolar discrete compounds and their solid solutions [1, 2], investigation of the systems becomes a challenge. The present article relates to investigation of thermal deformations of solid phases formed in a system composed of two essential amino acids: L-valine and L-isoleucine (Val—Ile).

This binary chiral system is unique due to the fact that molecules of its components have different numbers of chiral centers: a Val molecule ($C_5H_{11}NO_2$) has only one chiral center, while an Ile molecule ($C_6H_{13}NO_2$) has two. In addition, the system was found to produce the non-equimolar discrete compound V_2I [1]. This compound was detected and characterized in the course of a X-ray diffraction study of mixtures containing various proportions of Val and Ile. The mixtures were crystallized from aqueous solutions either by cooling or by isothermal evaporation. The compound V_2I is characterized by the molecular ratio Val:Ile = 2:1, and its crystal structure is layered as that of both Val and Ile, but differs from the latter by arrangement of the molecular layers. In case of Val and Ile the layers are azimuthally equivalent, while in case of V_2I those are azimuthally non-equivalent [1]. Accordingly, a comparative analysis of thermal deformations of the corresponding crystal structures of Val, Ile, and V_2I was performed.

Studies of thermal behavior of solid phases usually involve use of the differential scanning calorimetry (DSC) method. This method, however, is not applicable to the Val—Ile system, as its components decompose below melting point [3]. In present work, the temperature-resolved powder X-ray diffraction (PXRD) analysis was applied, which allowed to observe *in situ* thermal behavior of all the three phases and to perform a quantitative evaluation of thermal deformations of their crystal structure, i.e. to calculate parameters of thermal deformation tensor and to plot the figures of thermal expansion coefficients of corresponding crystal structures.

2 Experimental Methods

2.1 Studied materials

The initial reactants L(+)-Valine and L(+)-Isoleucine having 99 % purity were obtained from Alfa Aesar Company (Massachusetts, USA) and used as received. The reactants were applied to prepare the V_2I compound. It was crystallized from water via isothermal evaporation using Val and Ile in the ratio 2:1 (~66 mol % Val) as educts.

2.2 Analytical method: temperature-resolved powder X-ray diffractometry

The measurements were performed on a Rigaku Ultima IV diffractometer (Japan) provided with high-temperature equipment using $Cu_{K\alpha}$ radiation in air atmosphere. Temperature variation was from room temperature to the substance decomposition point with a temperature step of 10 or 20 °C. Computations of the X-ray diffractograms were performed using a STOE WinXPOW software package. Parameters of unit cell and tensor of thermal deformation were calculated using the programs UnitCell and DTC respectively.

3 Results and Discussion

3.1 Temperature dependences of monoclinic cell parameters of Val, Ile, and V_2I

Fig. 1 shows temperature dependences of the monoclinic cell parameters and the unit cell volume of the three discrete phases found in the system Val—Ile, i.e. the system components and the non-equimolar discrete compound V_2I. In case of Val and Ile the greatest elongation of the monoclinic cell is reflected by the parameter *c*, while in case of V_2I it is reflected by the parameter *a*.

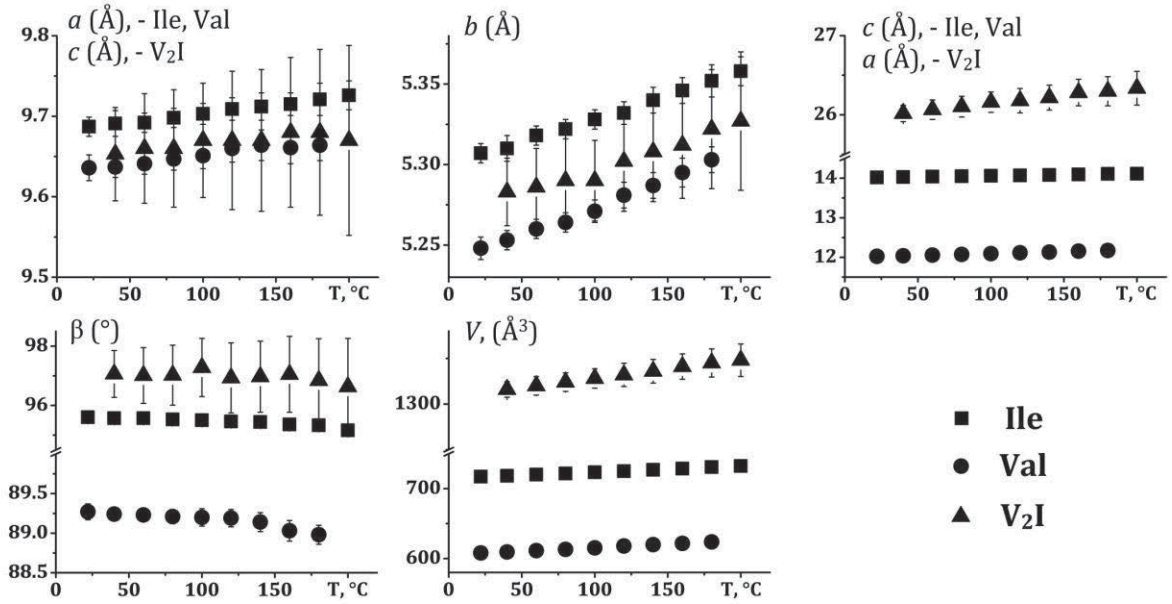

Fig. 1: Temperature dependence of parameters *a*, *b*, and *c* (Å), β (°), and volume *V* (Å³) of the monoclinic cell of Val, Ile, and V_2I. The symbols are identified in the figure.

The system components Val and Ile. While heated, Val and Ile do not undergo polymorph transformations. Their crystal structures incur only thermal deformations. The linear parameters *a*, *b*, and *c* (Å), and the volume *V* (Å³) of the monoclinic cell monotonically increase, while the angle β (°) monotonically decreases (see Fig. 1). Relative increases, or increments, of linear parameters and angle upon heating are different for Val and Ile. In case of Val the greatest increment (1.2 %) was observed for the parameter *c*,

while increment of the parameter *a* was the smallest (0.3 %). In case of Ile the parameter *b* was found to have the greatest increment (0.9 %), while the smallest increment was observed for *a* (0.4 %). Wherein, volumetric thermal expansion of the Val crystal structure (2.6 %) is considerably greater than that of Ile (2.0 %). It also should be noted that the Val decomposing point (205±5 °C) is somewhat lower than that of Ile (215±5 °C).

Non-equimolar discrete compound V_2I. Similar to Val and Ile, the discrete compound V_2I undergoes only thermal deformations: linear parameters and volume of its monoclinic cell monotonically increase, while the angle monotonically decreases (see Fig. 1). The greatest parameter *a* has the maximal increment (1.2 %), while the *c* parameter has the smallest (0.3 %). Additionally, volumetric thermal expansion of the V_2I crystal structure (2.5 %) is less than that of Val by 0.1 %, but exceeds the value obtained for Ile by 0.5 %. The decomposition temperature of the compound V_2I is very close to that of Ile (within ±5 °C) and exceeds the corresponding temperature of Val by ~10 °C.

The results of the temperature-resolved PXRD study were used for calculating parameters of thermal deformation tensors and for plotting the figures of thermal expansion coefficients for crystal structures of all the phases investigated.

3.2 Thermal deformations of the crystal structures of Val, Ile, and V_2I

It is to be kept in mind that crystal structures of Val, Ile, and the newly discovered discrete compound V_2I are layered [1]. The layers are composed of dimer molecules. Figs. 2a and 2b show dimer molecules of Val and Ile, respectively. In contrast to a Val molecule, one of the terminal H atoms is replaced by group CH_3 in the Ile molecule. The two molecules forming a dimer are connected by hydrogen bonds creating a “head-to-head” pattern in the crystal structure of each of the three compounds Val, Ile, and V_2I. Here the part of the molecule containing the NH_3 group is considered to be “the head”, and the opposite part of the molecule – to be “the tail”. Dimers arranged within a layer are interconnected by hydrogen bonds in the plane that is perpendicular to the longest axis of the monoclinic cell (see Figs. 3 and 4). The layer width across this plane is equal to the size of one dimer molecule. In Figs. 3 and 4, areas of hydrogen contacts are shadowed with dark grey color. Plurality of hydrogen bonds formed inside any dimer and between the dimers constitutes a network of hydrogen bonds within the layer. The hydrogen bond networks formed within the Val, Ile, and V_2I crystal structures do not possess substantial dissimilarities. The layers are interconnected by van der Waals bonds, which are shown as light grey gaps in Figs. 3 and 4.

Let us compare the projections of the figures of thermal expansion coefficient (TEC, or α) of the three relevant crystal structures on the planes *ac* (see Fig. 3) and *bc* (for Val and Ile) and *ba* (for V_2I) (see Fig. 4) of their monoclinic unit cells. Projections of TEC figures of all three compounds upon the *ac* plane have similar shapes. However, only Val and V_2I were found to have close values of the tensor parameters and similar orientations of the figure projections in relation to the axes of the monoclinic cell (see Figs. 3a, c). The Ile TEC tensor parameters calculated are significantly lower and also its degree of the figure rotation about the longest axis of the monoclinic cell is noticeably greater (see Fig. 3b). Projection of the Ile figure upon the *bc* plane has almost circular shape (see Fig. 4b), so it is rather different from ellipsoidal shapes of the corresponding projections of Val and V_2I figures (see Figs. 4a and 4c, respectively). At the same time, the Ile tensor parameters are considerably lower than those obtained for the tensors of Val and V_2I.

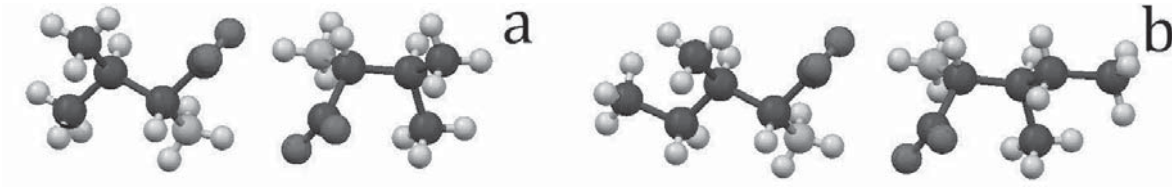

Fig. 2: Dimer molecules of Val (a) and Ile (b).
Atoms C, O, N, and H are colored in black, red, blue, and gray, respectively.

Despite a similar pattern of packing of the molecular layers in the crystal structures of Val and Ile, the differences in their thermal expansion are quite significant. On the other hand, while packings of the molecular layers in the crystal structures of Val and the discrete compound V_2I are different, the differences in their thermal expansion are not so prominent. The molecular layers in the Val crystal structure are packed azimuthally equivalently, while in the V_2I crystal structure – azimuthally non-equivalently [1]. Consequently, intensity of thermal expansion and thermal stability of the crystal structures of Val, Ile, and V_2I should be governed, first of all, by the interlayer van der Waals interactions, i.e. interactions between the molecular "tails".

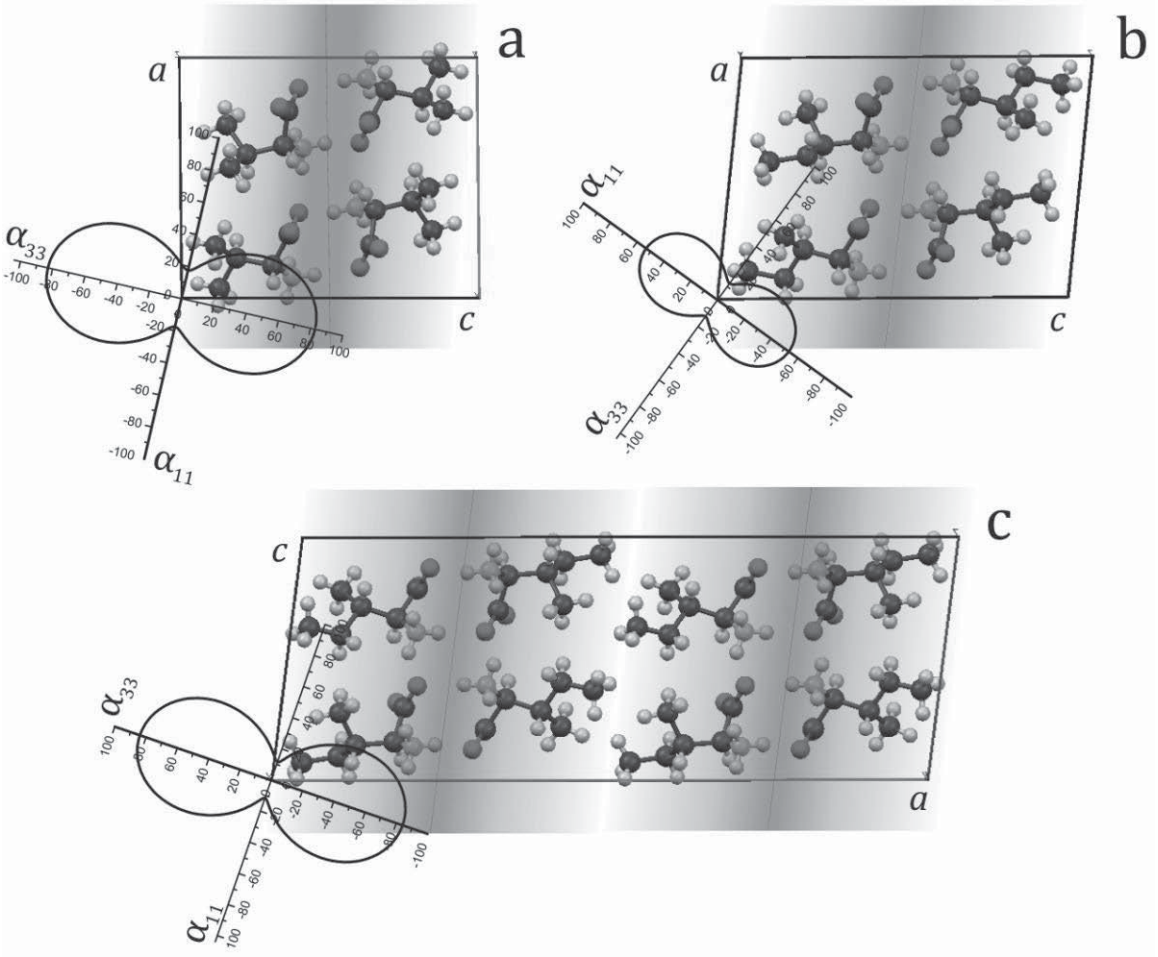

Fig. 3: Projections of the TEC figures upon the *ac* plane of the monoclinic cell of the crystal structures of Val (a), Ile (b), and discrete compound V_2I (c).
Explanations are provided in the discussion.

The presence of CH_3 groups in the tails of Ile molecules instead of H atoms in Val molecules results in an increase of the relative density of van der Waals contacts between the layers and, consequently, in strengthening the interlayer interactions. The occupation degree of corresponding positions in the molecule tails of Val, V_2I and Ile by CH_3 groups

is 0 %, 33 % and 100 %, respectively. These results account for the fact that thermal stability of V_2I is substantially lower than that of Ile and only slightly higher than thermal stability of Val. Accordingly, thermal expansion of V_2I and Val is characterized by much higher anisotropy than that of Ile.

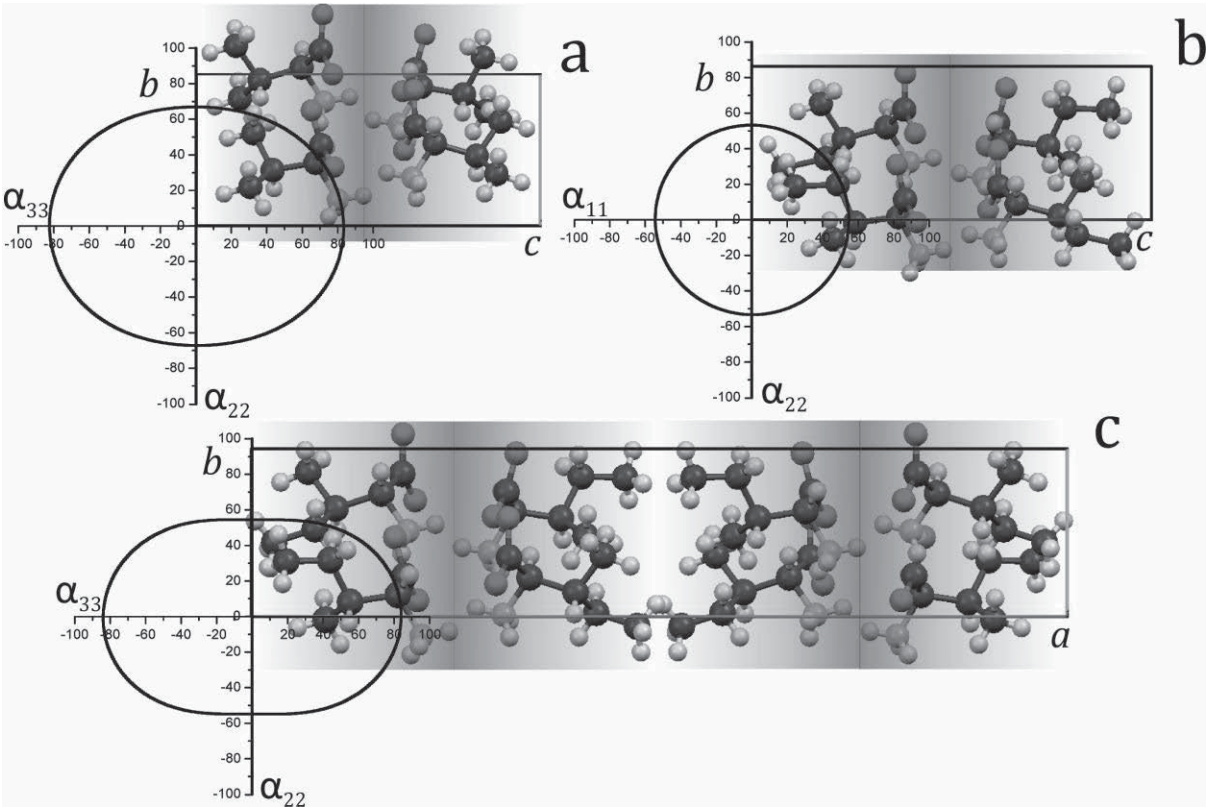

Fig. 4: Projections of the TEC figures of the crystal structures of Val (a) and Ile (b) upon the *bc* plane and of V_2I (c) upon the *ba* plane of their monoclinic cells. Explanations are provided in the discussion.

4 Conclusions

Temperature-resolved powder X-ray diffraction was used to study the thermal behavior of Val, Ile, and discrete compound V_2I. Each of these substances decomposes without being melted when heated in air. The decomposition temperatures of Val, Ile, and V_2I are 205±5 °C, 215±5 °C, and 215±5 °C, correspondingly. The compounds were studied to obtain results regarding their thermal deformations which included the determination of temperature dependences of the monoclinic cell parameters, the calculation of parameters of the TEC tensors, and also the plotting of the respective TEC figures. It was found that the crystal structure of Ile has the greatest thermal stability and the lowest volumetric thermal expansion among the three crystal structures studied, while the Val crystal structure, on the contrary, is characterized by the lowest thermal stability and the highest thermal expansion. Thermal stability of V_2I exceeds slightly that of Val, but is considerably lower than thermal stability of Ile. Accordingly, its thermal expansion significantly transcends that of Ile and slightly concedes that of Val. The data obtained were analyzed taking into account the concept of layered crystal structures of Val, Ile, and V_2I compounds. It was shown that differences in their thermal stability and intensity of their thermal expansion are controlled by van der Waals interactions between the layers of the dimer molecules, rather than intralayer hydrogen bonds. Moreover, the intensity of van der Waals interactions is defined by the relative density of contacts between the di-

mer molecules. The relative density of contacts, in turn, is defined by relative populating the tails of the contacting dimer molecules with CH_3 groups and H atoms.

References

(1) Isakov, A.; Kotelnikova, E.; Muenzberg, S.; Bocharov, S.; Lorenz, H. Solid Phases in the System L-Valine—L-Isoleucine. *Cryst. Growth Des*. **2016**, *16*, 2653–2661.
(2) Brandel, C.; Amharar, Y.; Rollinger J.; Griesser U.; Cartigny, Y.; Petit, S.; Coquerel G. Impact of Molecular Flexibility on Double Polymorphism, Solid Solutions and Chiral Discrimination during Crystallization of Diprophylline Enantiomers. *Mol. Pharmaceutics* **2013**, *10*, 3850–3861.
(3) O'Neil, M. J. *The Merck Index: An Encyclopedia of Chemicals, Drugs, and Biologicals*, 14; Merck & Co.: NJ, 2006.

Acknowledgements

The investigations were performed using equipment of the Saint Petersburg State University Resource Center "X-ray diffraction studies". The authors thank Dr. D. V. Spiridonova and Dr. M. G. Krzhizhanovskaya who made our experimental work in the center easier. The authors appreciate the financial support provided by the Russian Foundation for Basic Research (projects 16-05-00837 and 13-05-12053) and the Saint Petersburg State University Foundation (NIR 2/15, project 3.38.243.2015).

Influence of oiling out on the crystallization of L-menthol in water

Ian de Albuquerque[1] and Marco Mazzotti[1]

[1]ETH Zurich, Zurich, 8050, Switzerland
varela@ipe.mavt.ethz.ch

The crystallization of L-menthol in water was investigated, with the intent of comparing conventional crystallization with a crystallization process that enters liquid-liquid phase separation (LLPS). Within the scientific literature mixtures that undergo LLPS, loosely termed oiling out, are normally regarded as undesirable for a variety of reasons, such as, e.g., crystal purity, decrease in nucleation kinetics, and undesirable crystal size and shape, although few studies actually measure these quantities, particularly relating to crystal purities. It is the aim of this work to study the effects of LLPS on crystals, chiefly in terms of polymorphic form and crystal purity. The substance, L-menthol, was selected as it represents a relevant yet complex case, displaying four polymorphs and LLPS.

Initially, the phase diagram of L-menthol in water was measured, encompassing both solid-liquid (SLE) and liquid-liquid equilibrium (LLE). It was found that the solubility was very low, in the order of 0.04 wt.%, with a small temperature dependence. The monotectic temperature, i.e., when two liquid phases are in equilibrium with a solid phase, was measured and can provide a guide for process design.

To monitor the crystallization and oiling out process, Raman spectroscopy was selected due to its capability of probing the solid phase; measuring the liquid phase composition is not feasible due to the L-menthol's low solubility. A calibration between the Raman signal, at a specific wavenumber, and the solid suspension density was performed. Additionally, care was taken to select a wavenumber that would allow the quantitative identification of whether the vessel contains a solid suspension or a liquid-liquid mixture. This type of information is useful in estimating when the mixture enters LLPS and when it crystallizes.

Crystallization experiments that entered LLPS were performed as follows. Initially the solid suspension was maintained at 25°C for thirty minutes, followed by heating until 40°C, well above the monotectic temperature, and maintaining it at that temperature for another thirty minutes. Subsequently, the mixture was cooled until a final temperature, below the monotectic, so that crystallization would occur. The final crystals were collected and their polymorphic form assessed over time using DSC. What was observed is that initially the crystals obtained via oiling out were of a metastable polymorph and, over time, these crystals would transform into the stable form.

Finally, the crystals obtained from LLPS were shown to be anhydrous and free of solvent inclusions, and have comparable purities to the commercial material.

Stereoselective crystallization of enantiomers as a basis for chiral APIs production

A. Bredikhin

A.E. Arbuzov Institute of Organic and Physical Chemistry of Kazan Scientific Center of Russian Academy of Sciences, Arbuzov St., 8, Kazan 420088, Russian Federation
baa@iopc.ru

Direct methods of racemate resolution are deeply appreciated from fundamental and engineering point of view. We believe that their penetration into the routine practice would be facilitated through the widening of the really essential non-racemic compounds prone to spontaneous resolution in racemic form. It appears that the registered chiral active pharmaceutical ingredients (APIs) could be the objects of choice in this regard. During our systematic study of the properties of the terminal aromatic ethers of glycerol [1], we found that many of these compounds and/or their close structural analogues have a tendency to spontaneous resolution. Based on this property, we have developed direct methods of producing a wide range of registered single enantiomer APIs.

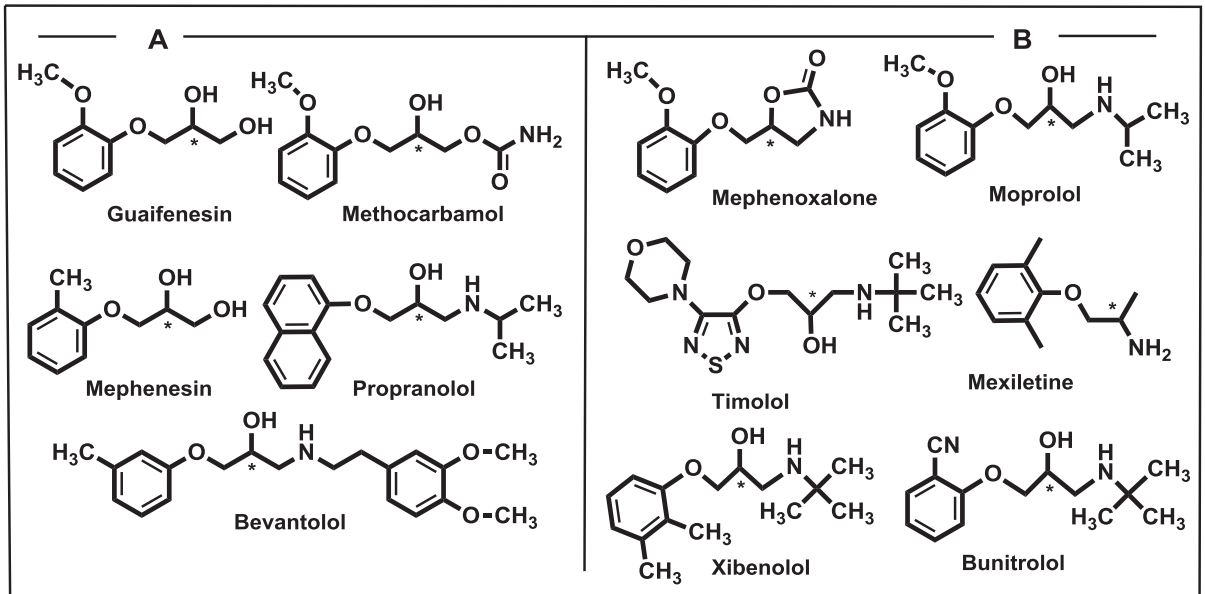

Some nonracemic APIs prepared using spontaneous resolution of the final products (A) or their synthetic precursors (B).

The report provides an overview of stereoselective crystallization of chiral APIs. We also discuss the well-known and our developed diagnostic of spontaneous resolution, as well as the ways to use the so obtained information in the development of efficient synthetic strategy for producing a target organic compounds in an enantiopure form.

The work was supported by the Russian Fund of Basic Research and Government of the Republic of Tatarstan within the framework of the research project No. 15-4302238.

(1) Bredikhin AA., Bredikhina Z.A., Zakharychev D.V. Crystallization of chiral compounds: thermodynamical, structural and practical aspects. *Mendeleev Commun*. **2012**, 22, 171-180.

The mechanism by which additives improve the preferential crystallization of L-asparagine monohydrate

P. Kongsamai[1], A. Maneedaeng[1], C. Flood[1], J. H. ter Horst[2], A. E. Flood[3]

[1]Department of Chemical Engineering, Suranaree University of Technology, Nakhon Ratchasima, Thailand
[2]EPSRC Centre for Innovative Manufacturing in Continuous Manufacturing and Crystallisation (CMAC), Strathclyde Institute of Pharmacy and Biomedical Sciences, University of Strathclyde, Glasgow, U.K.
[3]Department of Chemical and Biomolecular Engineering, School of Energy Science and Engineering, Vidyasirimedhi Institute, Rayong, Thailand

adrian.flood@vistec.ac.th

Preferential Crystallization (PC) is a popular process to separate enantiomers. The effectiveness of the process is limited by the nucleation and growth of the counter enantiomer during the process that can compromise the enantiopurity of the product. In previous research we have shown that the enantiomers of aspartic acid and glutamic acid can be used as inhibitors for the enantiomers of asparagine monohydrate (D- and L-Asn·H_2O). In this work we investigate the mechanism of the inhibition involved. The additives have no discernible effect on the solubility but had a small effect on the metastable limit, with additives tending to slightly widen the metastable zone but also make the zone widths more disperse. D-additives have a small effect on the growth rate of L-Asn·H_2O but L-Asp and L-Glu strongly inhibit the growth rate of L-Asn·H2O in DL-Asn·H_2O solution; there must also be a corresponding effect for D-Asp and D-Glu on D-Asn·H_2O. Population balance modeling of the batch preferential crystallizations was undertaken and can help to understand the mechanisms which change due to the presence of the additives.

1 Introduction

Preferential crystallization (PC) is a single step process that is easy and low cost for separating enantiomers. It achieves separation in a single process step through seeding the preferred enantiomer to the racemic supersaturation solution; the preferred enantiomer will crystallize at a higher rate than the counter enantiomer, and significant yield and enantiopurity can be achieved if the nucleation and growth of the counter enantiomer from the supersaturated solution can be avoided. PC has been applied to chiral species such as glutamic acid [1], asparagine [2], threonine [3] and methionine hydrochloride [4].
However, nucleation and growth of the counter enantiomer compromising the enantiopurity of the final crystalline product is a common problem in PC processes. The formation of the counter enantiomer can be slowed by the use of tailor-made additives to inhibit the crystallization of the counter enantiomer. Earlier research [5] has shown that enantiomers of aspartic acid and glutamic acid can inhibit the crystallization of the same-handed enantiomorphs of asparagine monohydrate (Asn·H_2O). This research investigates the mechanisms by which the additives inhibit the nucleation and growth of the counter enantiomer through the use of experimental measurements of the basic phenomena of nucleation and growth in solutions with and without additives and through the use of population balance model fitting of PC experiments. In this study, we use L-asparagine monohydrate (L-Asn·H_2O) as the preferred enantiomer in crystallization from DL-Asn·H_2O solutions.

2 Experimental Methods

2.1 Materials

DL-asparagine monohydrate (99+ wt%), L-asparagine monohydrate (99+ wt%) and D-asparagine monohydrate (99+ wt%), were purchased from Sigma-Aldrich. D-(-)-aspartic acid (99+wt%), D-(-)-glutamic acid (99+wt%), D-valine (98+wt%), D-leucine (99 wt%), L-(+)-aspartic acid (98+wt%), L-(+)-glutamic acid (99+wt%), L-valine (98+wt%), and L-leucine (99 wt%) were purchased from ACROS. These reagents were used without further purification. Deionized water was used as the solvent.

2.2 Solubility and metastable zone width

The solubility and the metastable zone limit of L-Asn·H_2O were determined using the Crystal16 (Technobis, Amsterdam). Samples were prepared with a known concentration of Asn·H_2O in 1 g of water. To determine the clear point temperature the suspension in the vial was heated with a heating rate of 0.1°C/min up to 60°C to complete dissolution. The temperature at which the turbidity reached zero was recorded. To determine the cloud point temperature the clear solution was subsequently cooled down to 2°C with a cooling rate of 0.1°C/min. The clear point temperature was taken as the saturation temperature of the solution while the cloud point was taken as the metastable limit of the solution for the cooling rate used.

2.3 Crystal growth experiments

Stock suspensions with various amounts of DL-Asn·H_2O in the presence and absence of various additives were prepared at 30°C and heated up to 58°C to completely dissolve the solute. Then the solution was cooled to the crystallization temperature, 30°C. Nine crystals of L-Asn·H_2O were attached by glue to a cover glass that was placed in a 50cm^3 small cell that was temperature-controlled using a jacket on the cell. The growth process began when solution was added to the cell. The size of the crystal was measured every 10 minutes until 80 minutes using a microscope and the DinoCapture 2.0 program. Concentration in the cell was analyzed using an automatic digital refractometer (RFM 340, Bellingham+Stanley Ltd., UK). We investigated the growth rate of L-Asn·H_2O crystals using supersaturation ratios (S) of 1.05, 1.10 and 1.15 for L-Asn·H_2O and DL-Asn·H_2O solutions. For investigation of the effect of additives we used 3 mol% of additives based on the total concentration of DL-AsnH_2O in solution at a supersaturation ratio (S) of 1.1.

2.4 Preferential crystallizations

Preferential crystallizations of L-Asn·H_2O (the preferred enantiomer) from DL-Asn·H_2O solutions with and without additives were performed. We prepared a solution of DL-Asn·H_2O with a supersaturation ratio (S) of 1.3 at 30°C in 40 g of water in a 50 mL crystallization vessel with jacket to control the temperature. Additives were added to the solution at 5 mol% compared to the total amount of DL-Asn·H_2O. The solution was heated to 50°C to completely dissolve the crystalline material. Subsequently, the solution was cooled down rapidly to the crystallization temperature of 30°C. L-Asn·H_2O seeds, 0.02 g (300-500micron) were added into the solution the moment the crystallization temperature reached at 30°C. The process was stopped at a given time and the suspension was filtered to obtain crystal samples at different times from 1 h to 7 h after the addition of seeds. The solid product was kept in a desiccator for drying. The solid products were analysed by HPLC (1260 Infinity, Agilent Technologies) with a Chirobiotic T column. The HPLC analysis was performed at 25°C using a 70:30 vol% ethanol: water mixture as a mobile phase and using UV detection at 205 nm. The injection volume was 5 µL.

2.5 Process Modeling and Model Fitting

The preferential crystallization of L-Asn·H_2O was modeled using the moment form of the population balance. The relevant equations for the preferred enantiomer are

$$G_L = k_{G,L}(S_L - 1)^{n_{G,L}}$$

$$J_{L,2nd} = k_{J,L}(S_L - 1)^{n_{J,L}} C_L^{n_2}$$

$$\frac{\mu_{L,0}}{dt} = \begin{cases} J_{L,2nd} & if \;\; S_L > 1 \;\; and \; t \geq t_{ind} \\ 0 & if \;\; S_L \leq 1 \end{cases}$$

Where C represents suspension density. The population balance (in the moment form) is

$$\frac{d\mu_{L,j}}{dt} = jG_L\mu_{L,j-1} \quad j = 1,2,3, \ldots$$

The equations for the counter enantiomer are similar;

$$G_D = k_{G,D}(S_L - 1)^{n_{G,D}}$$

$$J_D = k_{J,D}(S_D - 1)^{n_{J,D}}$$

$$\frac{\mu_{D,0}}{dt} = \begin{cases} k(S_D - 1)^n & if \;\; S_D > 1 \;\; and \; t \geq t_{ind} \\ 0 & if \;\; S_D \leq 1 \end{cases}$$

$$\frac{d\mu_{D,j}}{dt} = jG_D\mu_{D,j-1} \quad j = 1,2,3, \ldots$$

These equations were used with mass balances on the two solutes. The parameters in the models were fitted by minimizing differences between the predicted and experimental data points for the preferential crystallization experiments. In experiments with additives there is no requirement for the parameter values for the D- and L- enantiomorphs to be identical.

3 Results and discussion

3.1 Solubility, metastable zone and crystal growth

Solubility and metastable zones of pure enantiomorphs and racemic mixtures of asparagine monohydrate are shown in Fig. 1. Results are shown for both pure solutions and solutions containing amino acid additives at 5 mol%. The results show that the additives had no significant on the solubility, however they tended to make the zone width more disperse without modifying the average zone width.

Crystals of L-Asn·H_2O grown from aqueous solution are shown in Fig. 2. The crystal growth rate is based on the principle axis. The growth rate is modified to a spherical average growth rate when used in the population balance. Plots of crystal growth are shown in Fig. 3. Crystal growth rates in solutions without additives are shown in Table 1, and in solution containing additives in Table 2.

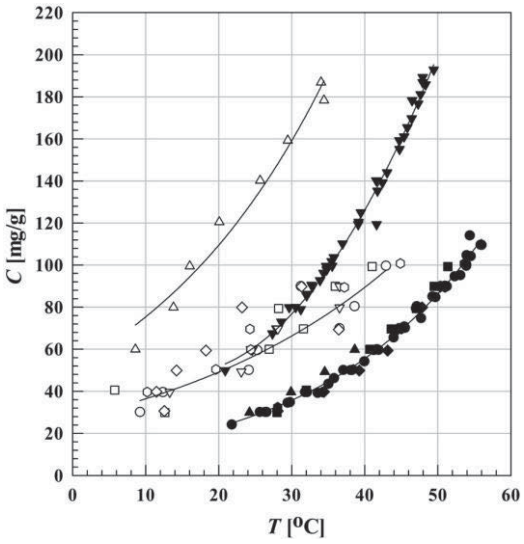

Fig. 1: Solubility and metastable zone widths. Solubility points consist of L-Asn·H_2O (●), DL-Asn·H_2O (▼), D-Asn·H_2O with D-Asp (■), D-Asn·H_2O with D-Leu (◆), D-Asn·H_2O with D-Glu (▲), L-Asn·H_2O with D-Val (⬢), and cloud points consist of L-Asn·H_2O (○), DL-Asn·H_2O (△), D-Asn·H_2O with D-Asp (□), D-Asn·H_2O with D-Leu (◇), D-Asn·H_2O with D-Glu (▽), and D-Asn·H_2O with D-Val (⬡).

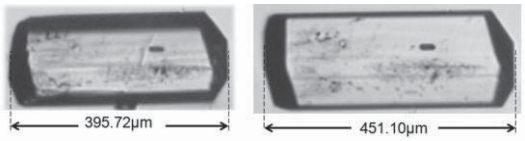

Fig. **2**: Crystals of L·Asn.H2O.

Table 1. Parameters for the crystal growth rate distributions for asparagine monohydrate.

S	L-Asn·H_2O solution			DL-Asn·H_2O solution		
	1.05	1.1	1.15	1.05	1.1	1.15
G_o (µm/min)	0.51	0.96	1.41	0.29	0.60	0.89
σ_G	0.09	0.11	0.12	0.07	0.11	0.18
R^2	0.9972	0.9835	0.9360	0.9985	0.9423	0.9765

Table 2. Parameters for the crystal growth rate of asparagine monohydrate using additives.

Type of additives	no additives	D-Asp	D-Glu	D-Leu	D-Val	L-Asp	L-Glu	L-Leu	L-Val
G_o (µm/min)	0.60	0.39	0.47	0.69	0.60	0.19	0.28	0.62	0.73
σ_G	0.11	0.07	0.09	0.11	0.08	0.06	0.06	0.12	0.07
R^2	0.9423	0.9903	0.9995	0.9824	0.9844	0.9643	0.9974	0.9829	0.8964

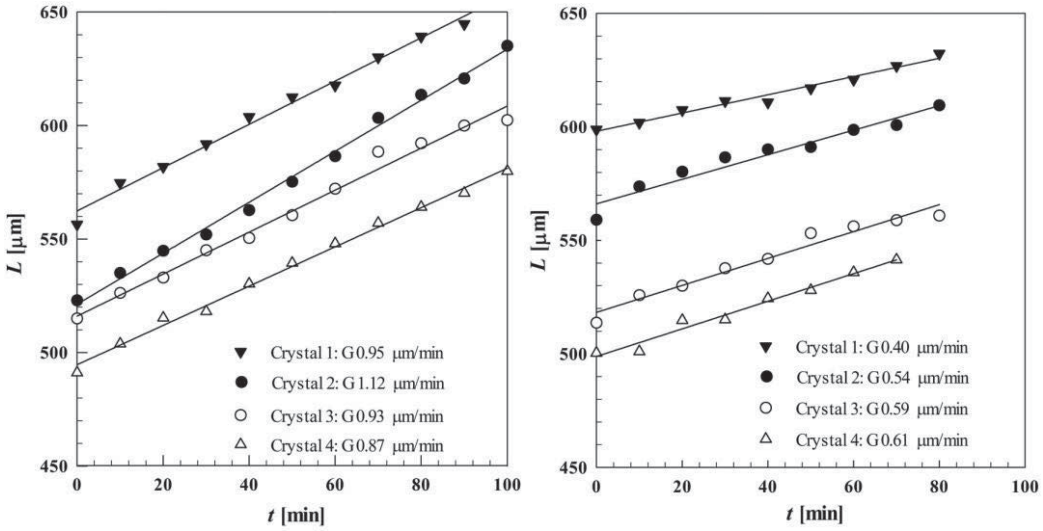

Fig. 3: Crystal growth rates of samples of L·Asn.H_2O crystals in solutions of L-Asn (left) and DL-Asn (right).

3.2 Preferential crystallizations of asparagine monohydrate

Results for the preferential crystallizations with and without additives are shown in Fig. 4. It is clear that some additives, particularly aspartic acid and glutamic acid are suitable to extend the crystallization time before the counter enantiomer nucleates (or crystallizes to an appreciable level).

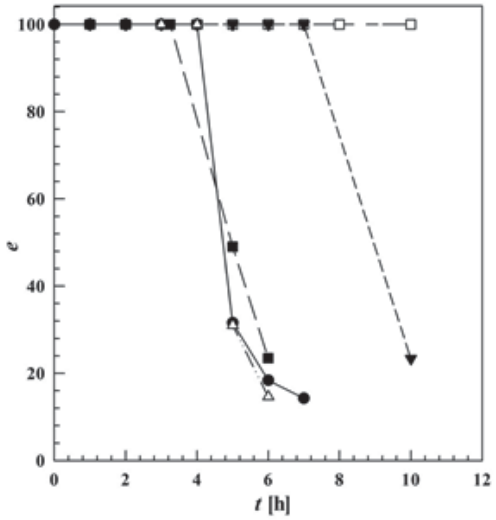

Fig. 4: The enantiomeric excess *e* of L-Asn·H_2O in the crystal phase during a preferential crystallization (PC) of L-Asn·H_2O from DL-Asn·H_2O in water in absence of additives (●), with 5% mol of D-Asp (□) with 5% mol of D-Glu (▼), with 5% mol of D-Val (△), with 5% mol of D-Leu (■).

3.3 Model fitting of the experimental data

Some data needed for the population balance modeling are already known from the base experiments done earlier including crystal growth rate experiments and induction time measurements. In particular, in systems with no additives the growth rate equations used were $G_{D-} = G_{L-} = 4.863x10^{-8}(S - 1)$ (m/s). The induction time for the system with no additives was estimated from measured induction times. Initial conditions used (for instance the first four moments of the seeds and the initial concentrations and temperature) were taken from the initial conditions of the experiments. This leaves only nuclea-

tion rates to be determined through fitting of the experimental data. Potentially these values could be estimated using the metastable zone widths, however our experience with estimates of nucleation rates from zone width data is poor and hence we have fitted using experimental data. The models includes both primary and secondary nucleation. Primary nucleation is certainly necessary for the counter enantiomer (and therefore must also occur in the case of the preferred enantiomer) else it could not crystallize. Both enantiomorphs may also nucleate via secondary nucleation, the rate of which is dependent on the suspension density of the component being considered. The nucleation models determined for the system without additives are

$J_i = 290 \times 10^3 (S-1)^{0.136}$ for primary nucleation

$J_{i,2nd} = 273 \times 10^3 (S-1)^{1.717} C_i^{0.52}$ for secondary nucleation.

Using the same models for systems where there are additives allows the determination of which kinetic mechanisms are being affected by the additives, and therefore how the additives assist in the preferential crystallizations.

4 Conclusions

Successful preferential crystallizations have been performed for asparagine monohydrate, both with and without additives. Amino acid additives can inhibit the enantiomer of the same handedness as the additive, particularly the additives glutamic acid and aspartic acid. The results can be understood based on careful experiments of the basic phenomena involved (solubility, induction time, zone width,…) and population balance modeling to extract kinetic data which is difficult to obtain from these experiments, in particular nucleation rates via primary and secondary nucleation.

References

(1) Buhse, T., Kondepudi, D. K. Hoskins, B. Kinetics of chiral resolution in stirred crystallization of D/L-glutamic acid *Chirality* **1999**, 11, 343-348.
(2) Petruševska-Seebach, K.; Seidel-Morgenstern, A.; Elsner, M. P. Preferential Crystallization of L-Asparagine in Water *Cryst. Growth Des*. **2011**, 11, 2149-2163.
(3) Profir, V. M., Matsuoka, M. Processes and phenomena of purity decrease during the optical resolution of dl-threonine by preferential crystallization *Colloid Surface A,* **2000**, 164, 315-324.
(4) Srimahaprom, W., Flood, A. E. Crystal growth rates and optical resolution of dl-methionine hydrochloride by preferential crystallization from aqueous solution *J. Cryst.* Growth **2013**, 362, 88-92.
(5) Kongsamai, P., Maneedaeng, A., Flood, A.E., ter Horst, J.H. Processes and phenomena of purity decrease during the optical resolution of dl-threonine by preferential crystallization. In International Symposium on Industrial Crystallization (ISIC19th), **2014**.

Acknowledgements

PK thanks the Thailand Research Fund through the RGJ Ph.D. fund for support of this research.

Phase behavior of a chiral agrochemical as basis for crystallization based separation

A.-K. Kort[1], H. Lorenz[1], A. Seidel-Morgenstern[1,2]

[1]Max Planck Institute for Dynamics of Complex Technical Systems, Magdeburg, Sachsen-Anhalt, 39106, Germany;
[2]Otto-von-Guericke University, Magdeburg, Sachsen-Anhalt, 39106, Germany;
korta@mpi-magdeburg.mpg.de

Enantioseparation by crystallization is an effective method to obtain pure enantiomers out of their mixtures. The acquirement of physical-chemical data and the corresponding phase diagrams is fundamental for the design of a crystallization process. For organic substances possessing a low melting point during crystallization oiling out often occurs. Thus, identification of the liquid-liquid phase boundaries is essential to find a proper operation window for a successful crystallization. In this contribution polythermal and isothermal methods are applied to examine phase diagrams on the example of chiral Mefenpyr-diethyl.

1 Introduction

Chirality becomes more and more important in the agrochemical industry, since more than 25% of the known pesticides contain chiral centers [1]. By reason of differentiation of receptors between enantiomers in biochemical interactions, dissimilarities of activity of each enantiomer might be caused.

In previous studies we investigated the feasibility of a 2-step-preferential crystallization process for enantiopurification of the chiral fungicide Fenamidone. Binary and ternary phase diagrams were examined and used for crystallization based enantioseparation of the racemate [2, 3].

In this work the crystallization behavior of another chiral agrochemical substance, namely Mefenpyr-diethyl, is studied (Fig 1). Mefenpyr-diethyl is a safener often combined with herbizides, such as Fenoxaprop-P-ethyl or Iodosulfuron. Because of slight toxicity and a value of $log\ P_{OW} = 3.83$ (pH = 6.3, $T = 21$ °C) this substance offers an improvement of cultural compatibility [4, 5]. Possessing an imidazol-heterocycle, benzene

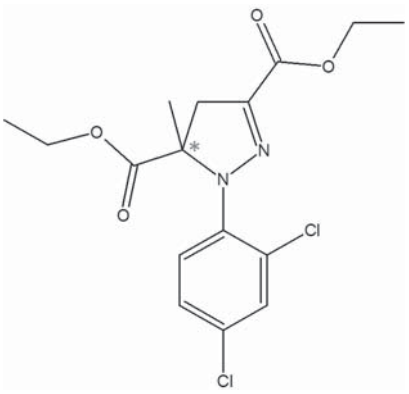

Fig. 1: Chemical structure of racemic Mefenpyr-diethyl.

derivatives and a stereocenter, this molecule shows complexity in its structure. Since Mefenpyr-diethyl is forming a racemic compound, enantioseparation by crystallization

is more difficult in comparison to reported strategies for separation of conglomerates [6, 7].

The racemic compound and the enantiomers of Mefenpyr-diethyl reveal relatively low melting temperatures with ≈ 50 °C and ≈ 30 °C, respectively. In case of substances having a low melting temperature and also in presence of an antisolvent, oiling out often occurs. Such a liquid-liquid phase separation (LLPS) during a crystallization process from a solution is caused by a miscibility gap in liquid state [8, 9], characterized by the presence of a solute-rich and a solute-poor liquid phase. Since the solute-rich phase often is a good "'solvent"' for impurities, LLPS prior to the crystallization is undesired [10]. Therefore the knowledge of the phase diagram including possible miscibility gaps and the exact identification of the related phase boundaries are necessary for the design of successful crystallization processes.

2 Experimental Methods

2.1 Materials

Racemic Mefenpyr-diethyl was provided by BayerCropScience AG with purity of 99.3 %. Small amounts of pure enantiomers (99.9 ee%) were separated out of the racemic material by use of preparative high performance liquid chromatography (PHPLC; column: ChiralCel OJ; mobile phase: n-hexane/ethanol/methanol (85/7.5/7.5); flow: 75 $ml \cdot min^{-1}$). Ethanol was purchased from VWR (99.6 %) and water was distilled and deionized applying Milli-Q® (Merck Millipore, Germany).

2.2 Solubility measurements

Solubility measurements were performed using common isothermal solubility equipment. Since solubility in pure ethanol is high ($c_{EtOH} \geq 20$wt% at 10 °C to 20 °C) water is used as an antisolvent [5]. Suspensions of 1.5 ml Mefenpyr-diethyl in ethanol/water mixtures were equilibrated under stirring for 48 h. An additional experiment revealed an equilibration time of approximately 18 h. After reaching equilibrium three samples of the saturated solution were withdrawn using a syringe together with a syringe filter. The concentration was subsequently analyzed gravimetrically. Isothermal solubility measurements were done for racemic compound and enantiomer of Mefenyr-diethyl between 0 °C and 20 °C in ethanol/water mixtures of composition 80/20 and 70/30, respectively. During isothermal solubility measurements LLPS was detected at specific concentrations and temperatures.

2.3 Detection of LLPS boundaries

2.3.1 Polythermal studies

To determine temperature dependencies of LLPS in ethanol/water mixtures experiments of small scale were performed applying the parallel crystallizers Crystal16® (0.5 ml to 1 ml) and Crystalline® (3 ml to 5 ml) (Technobis, Netherlands). Solutions of known compositions and concentrations were first heated to obtain a homogeneous mixture, cooled in a further step until turbidity is detected (cloud point) and afterwards heated again as far as the turbidity becomes zero (clear point).

In case of similar temperatures of clear and cloud points LLPS appears, while an SLE would exist if an obvious difference between both characteristic temperatures is found, since the rate of formation of the oily droplets is faster than crystal formation [11]. Additionally, types of existing phases were identified optically with the help of a microscopic camera (see Fig. 2).

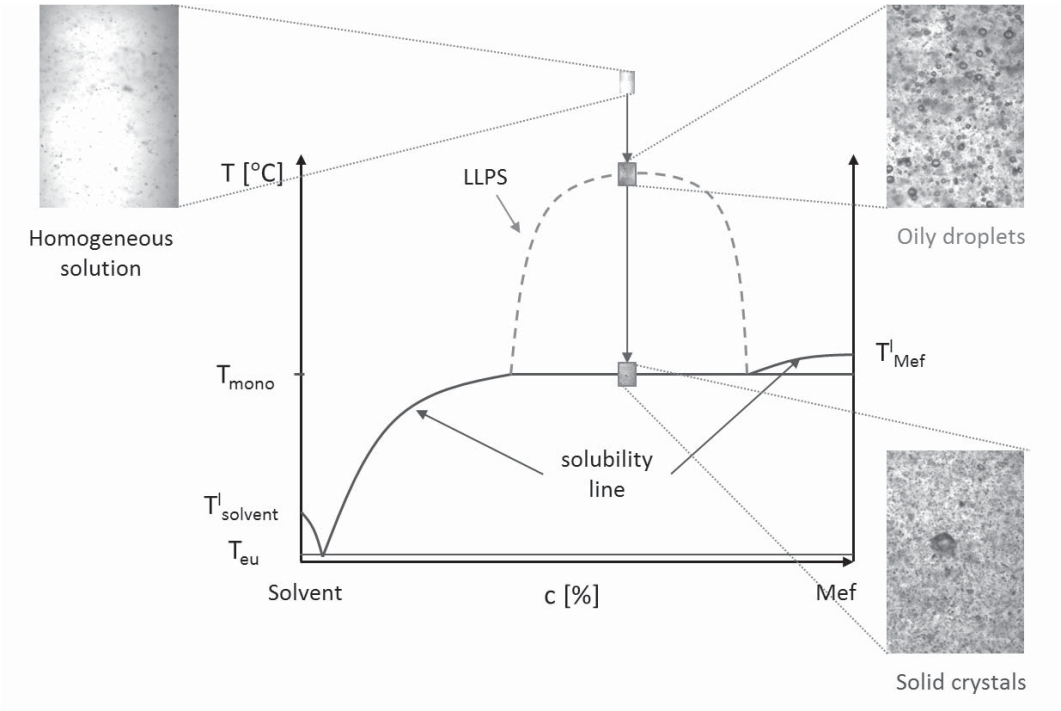

Fig. 2: Scheme of polythermal detection of LLPS boundaries in the Mefenpyr-diethyl/solvent system (Mef – Mefenpyr-diethyl).

For investigation of monotectic temperature (T_{mono}) prepared samples of a certain concentration were stepwise cooled to the temperature range where formation of a solid phase was expected, using slow cooling rates ($0.05\ \mathrm{K \cdot min^{-1}}$) and long retention times of 5 h at single temperatures (intervals of 1 K). Since the monotectic temperature must be lower than the melting temperature of the pure substance, anticipation of a certain temperature range was given. In case of Mefenpyr-diethyl this bandwidth is figured between 20 °C and 30 °C for the enantiomer and 30 °C and 50 °C for the racemic compound. Again, optical phase behavior (solidification) was monitored by microscopic cameras in the Crystalline® instrument (Fig. 2).

2.3.2 Isothermal studies

Since polythermal obtained temperatures are not that precise and to quantify the LLPS boundaries in the phase diagram, isothermal investigations were performed using a ThermoMixer® equipment (Eppendorf). Small scale samples (1 ml) of racemic Mefepyr-diethyl in ethanol/ water mixtures (40 - 60 wt% of Mefenpyr-diethyl) were shaken for 24 h at a certain temperature between 30 °C to 70 °C. After reaching equilibrium the two liquid phases were separated using a pipette and analyzed gravimetrically. The solute-poor phase and the solute-rich phase specify the boundaries of the LLPS region at the respective temperature (see Fig 3).

3 Results and Discussion

3.1 Solubility diagrams

Fig. 4 shows solubility diagrams of Mefenpyr-diethyl enantiomer and racemic compound in ethanol/water mixtures of composition 80/20 and 70/30, respectively. As can be seen, solubility increases with rising temperature. Solubilities of the enantiomer are

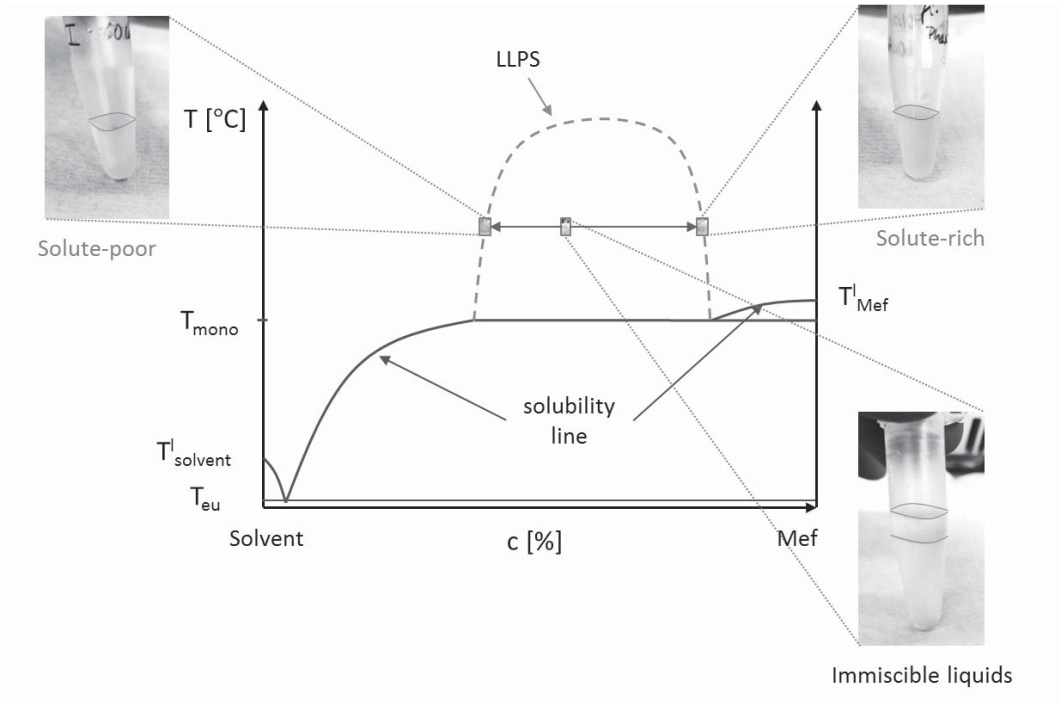

Fig. 3: Scheme of isothermal analysis of two occurring liquid phases in the Mefenpyr-diethyl/solvent system (Mef – Mefenpyr-diethyl).

higher than those of the racemic compound at all temperatures in both solvent mixtures. The solubility differences in ethanol/water 80/20 are $\Delta c = 4$ wt% at 20 °C and in ethanol/water 70/30 at the same temperature $\Delta c = 5$ wt%. At 0 °C the saturation concentration of the enantiomer in ethanol/water 80/20 is 3.9 wt% higher than the saturation concentration of the racemic compound, while this difference has a value of 1.2 wt% in ethanol/water 70/30.

Since water is an antisolvent in the system, the saturation concentration in ethanol/water 70/30 is continually lower than in ethanol/water 80/20. For instance at 10 °C the concentration difference for the racemate is 3.9 wt% and at 20 °C the difference is 5.3

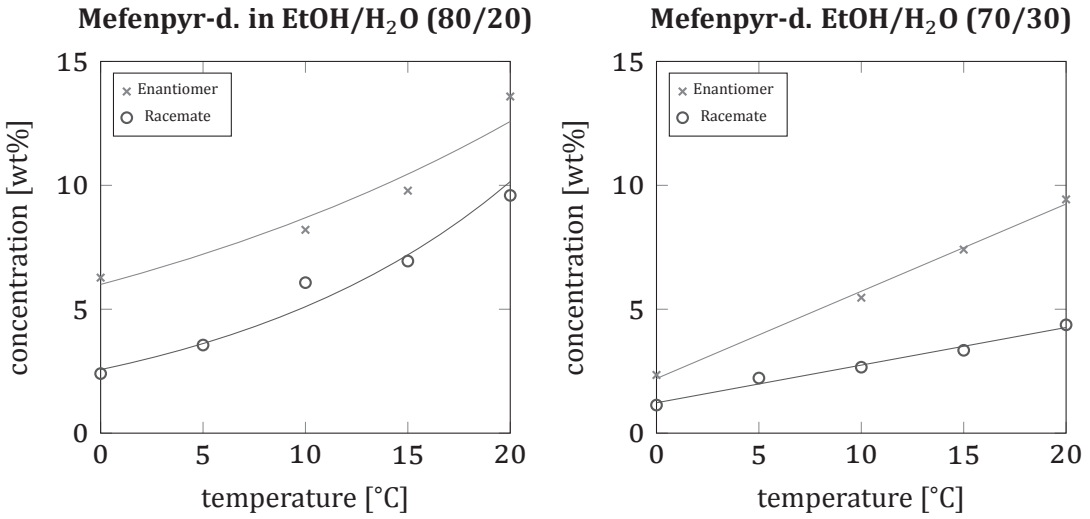

Fig. 4: Isothermal solubility diagrams of Mefenpyr-diethyl enantiomer and racemic compound in ethanol/water mixtures 80/20 and 70/30.

wt%. It is clear from the data that the solubility lines at higher ethanol content offer a steeper increase of saturation concentration. Because of the higher solubility values and the stronger slope of the solubility curve, crystallization in ethanol/water 80/20 as solvent should provide higher yields working in the same temperature range.

3.2 Detection of LLPS boundaries and conclusions

Solubility measurements were run under isothermal conditions in a temperature range between 0 °C and 20 °C. The determination of oiling out boundaries could be achieved in a small scale (0.5 ml to 5 ml) applying the reported polythermal and isothermal methods. First data points in the LLPS region have been successfully determined. Further results will be published soon. In future, the determination of the entire phase diagram will be performed. Finally, crystallization strategies for enantioseparation of the racemic compound should be derived considering Preferential Crystallization.

References

(1) Ulrich, E. M.; Morrison, C. N.; Goldsmith, M. R.; Foreman, W. T., *Chiral Pesticides: Identification, Description, and Environmental Implications*; Springer US: 2012.

(2) Kort, A.-K.; Lorenz, H.; Seidel-Morgenstern, A. Resolving mixtures of enantiomers of two agrochemicals. *Proceedings 22nd Int Workshop on Industrial Crystallization (BIWIC 2015)* **2015**.

(3) Kort, A.-K.; Lorenz, H.; Seidel-Morgenstern, A. Physical-chemical Properties of the Chiral Fungicide Fenamidone and Strategies for Enantioselective Crystallization. *Chirality* **2016**, *28*, 514–520.

(4) Schirmer, U.; Jeschke, P.; Witschel, M., *Modern Crop Protection Compounds: Herbicides*; Bd. 1; Wiley-VCH Verlag: 2012.

(5) Hacker, E.; Bieringer, H.; Willms, L.; Roesch, W.; Koecher, H.; Wolf, R. Mefenpyr-diethyl: Ein Safener fuer Fenoxaprop-P-ethyl und Isosulfuron in Getreide. *Z. Pfl-Krankh. PflSchutz, Sonderh.* **2000**.

(6) Coquerel, G., *Preferential Crystallization*; Springer-Verlag Berlin Heidelberg: 2006.

(7) Lorenz, H.; Seidel-Morgenstern, A. Processes To Separate Enantiomers. *Angew. Chem Int. Ed.* **2014**, *53*, 1218–1250.

(8) Tung, H.; Paul, E.; Midler, M.; McCauley, J., *Crystallization of Organic Compounds: An Industrial Perspective*; Wiley: 2009.

(9) Lorenz, H. In *Crystallization*, Beckmann, W., Ed.; Wiley-VCHVerlag: 2013; Chapter 3, pp 35–74.

(10) Deneau, E.; Steele, G. An In-Line Study of Oiling Out and Crystallization. *Org. Process Res. Dev.* **2005**, *9*, 943–950.

(11) Ricci, J., *The Phase Rule and Heterogeneous Equilibria*; Van Nostrand: 1951.

Acknowledgements

Thanks for help go to Professor Ernst R. Gesing at BayerCropScience AG for providing material of example substances Fenamidone and Mefenpyr-diethyl.

Temperature-cycling-induced Deracemization of a Racemic Compound via its Conglomerate Salt

W. Li[1], Herman J.M. Kramer[1], J.H. ter Horst[2]

[1]Process and Energy department, Delft University of Technology, Delft, 2628CB, the Netherlands;
[2]EPSRC Centre for Innovative Manufacturing in Continuous Manufacturing and Crystallisation (CMAC), Strathclyde Institute of Pharmacy and Biomedical Sciences, Technology and Innovation Centre, 99 George Street, Glasgow G1 1RD, United Kingdom
w.li-1@tudelft.nl

Heating-cooling cycles coupled with solution phase racemization were proven to be a powerful alternative to grinding in the deracemization of a racemic suspension. However, the application of both techniques is limited to chiral molecules which crystallize as conglomerates, mechanical mixtures of enantiopure crystals of either enantiomer. This restriction excludes more than 90% of the known chiral compounds from direct deracemization as they all crystallize as racemic compounds, crystals in which both enantiomers are homogeneously distributed. In order to loosen this restriction, the conversion from racemic compounds to conglomerates is needed.
Phenylalanine (Phe), for instance, crystallizes as racemic compounds but can be converted into a conglomerate salt by using the base 2,5-Xylenesulfonic acid (XSA). Through this conglomerate salt we could obtain enantiopure Phe in the form of the salt using temperature cycling induced deracemization, assisted by a solution phase racemization reaction catalysed by salicylaldehyde. In the verification experiment, starting from a racemic suspension of Phe-XSA in acetic acid, 100% solid phase enantiomeric excess was achieved within 350 hours using temperature-cycles between 65°C and 70°C. To the best of our knowledge, the temperature-cycle-induced deracemization of a conglomerate forming salt has never been reported. In addition, a preliminary comparison between the deracemization rate constants of the salt by Viedma Ripening and temperature cycling indicated that the latter one is a more efficient technique to obtain the desired chiral purity in the industry.
Subsequently, the effect of operation conditions on the deracemization rate constant were investigated. The catalyst concentration for the racemization reaction significantly increases the deracemization rate. This might be due to the increase of the salt solubility with the catalyst concentration. Both the suspension density and the temperature profile control the mass fraction of solid involved in the dissolution-growth cycle, which showed a linear relationship with the cycle-based deracemization rate constants.
Finally, a population balance model emphasizing the differences in dissolution and growth kinetics of the two enantiomers was developed, predicting the enantiomeric excess development during a temperature cycle. Particle Size Distribution (PSD) and enantiomeric excess changes over the course of temperature cycles were measured and compared with the simulated ones. The modelling is applied to verify possible mechanisms for the temperature cycling induced deracemization.

